Fibers and Polymers 2018, Vol.19, No.3, 599-606
DOI 10.1007/s12221-018-7937-1

ISSN 1229-9197 (print version)
ISSN 1875-0052 (electronic version)

Perspective on Carbon Fiber Woven Fabric Electrodes for Structural Batteries

Mi Young Park[1], Joo-Hyung Kim[2], Do Kyung Kim[2], and Chun Gon Kim[1]*

[1]*Department of Aerospace Engineering, School of Mechanical and Aerospace Engineering, KAIST, Daejeon 34141, Korea*
[2]*Department of Materials Science and Engineering, KAIST, Daejeon 34141, Korea*

(Received November 5, 2017; Revised January 24, 2018; Accepted January 28, 2018)

Abstract: The purpose of this work is to explore effective means of fabricating nanostructure-deposited continuous woven carbon fabric and to investigate the feasibility of using this material in structural battery applications. In order to prove this concept, two types of nanostructured carbon fabric electrodes – one with vertically-aligned carbon nanotubes (VACNTs) formed directly on carbon fabric utilizing iron (Fe) nanoparticles and Al buffer layers, the other with the same VACNTs on a chemical vapor-deposited graphene surface utilizing Ni seed layers on the carbon fabric – were fabricated to investigate material electrical performances as battery electrodes. The reversible specific capacity of 250 mAh/g on average at C/20 with good cyclic retention in these three all-carbon electrodes, including pristine carbon fabric, suggests a promising structural battery electrode for low-current battery applications. Even though the capacity of VACNT-grafted carbon fabrics was limited due to poor wetting of the VACNT forest with electrolyte caused by the lack of functionalization of the VACNT, their excellent cyclic performances and galvanostatic curves support the idea that the carbon nanotube and carbon fabric combination can be utilized in battery applications. However, pristine-carbon fabric is still a good candidate for battery applications because of its simplicity of mass production.

Keywords: Carbon fabric electrode, Nanostructured carbon fabric, Carbon nanotubes, Structural battery, Cyclic performance

Introduction

The low gravimetric weight and low volume of CNT and graphene-nanostructures can cause an increase of energy density when CNTs are coated on cabon fabric by enabling good electrical and mechanical contact. Vertically-aligned carbon nanotubes (VACNTs) on metal substrates are useful in diverse applications such as highly sensitive electrochemical biosensors, electron emitters of field emission devices, high-performance fuel cell devices, and supercapacitors; this is because VACNTs have high electrical conductivity, and large surface-to-volume ratio, as well as good chemical inertness, and high mechanical strength [1-8]. Direct growth of graphene and CNT on carbon fabric has been reported in investigations of ultra-high density exposed graphene edge planes that retain the porous structure of CNTs on carbon paper as an all-carbon G-CNT hybrid structure for enhanced proton exchange membrane fuel cells (PEMFC) [9]. Commercially-available carbon fabric has been reported in research into potential uses of multifunctional structural supercapacitors and batteries [10-14]. All these investigations can be integrated into the study of efficient-energy-storing multifunctional structures, such as a structural batteries. The objective of the present research is to investigate the electrical characteristics of nanostructure-coated carbon fabric for energy structure applications such as structural battery electrodes. In order to explore an effective means of application and to verify the concept, we considered first the chemical vapor deposition (CVD) process as one of the most commonly used methods of growing CNTs for the fabrication process of nanocomposite structural electrodes and studied the best growth mechanism of carbon nanostructures on carbon fabric substrates. The results were then used to compare and evaluate the performance of battery electrodes made of pristine carbon fabric to that of nanostructured electrodes.

*Corresponding author: cgkim@kaist.edu

Experimental

Conceptually, a structural battery is comprised of a solid- or quasi-solid-based polymer electrolyte with a load-carry function; continuous carbon fabric preforms can take the shape of a laminate with a polymer-supported matrix. This concept requires that the carbon fiber reinforcement have an electrochemical function of battery electrode as well as a-reinforcement with high mechanical strength. In order to satisfy this concept, our preliminary design purpose of the carbon fiber electrode is to verify that carbon fiber woven fabric layers can function as an electrode, i.e. that it can intercalate ions into its carbonaceous structure. For verification of this idea, we attempted to determine appropriate fiber surface morphologies for effective electrode function and evaluated the battery performance using standard electrochemical testing and analysis methods. Three types of electrode morphologies were considered for a-battery performance evaluation: a pristine carbon fabric, and two nanostructured carbon fabrics, one comprised of CNTs only and the other of CNTs with graphene-deposited carbon fabrics-(G-CNT-CF). The CNT-carbon fabric electrode is denoted as CNT-CF; the graphene-CNT-carbon fabric

electrode is denoted as a G-CNT-CF. The pristine carbon fabric electrode is called the pristine-CF electrode.

The design of the two nanostructure-coated electrodes is meant to enhance the electrical capacity by growing VACNTs and retaining good mechanical contact between nanostructure layers, compensating for carbon fabric's surface roughness.

Materials

Plain woven carbon fiber fabric electrodes: PAN-based carbon fiber fabric was used in plain weave, TR30 (Profil™ TR30S), from Mitsubishi Rayon Co., Ltd., with a normal thickness of 130 μm, areal density of 1.795 g/cm^2, fiber tensile strength of 4,354 MPa, and tensile modulus of 235 GPa. The carbon fabric was used as received, and no activation or pretreatment was conducted before initial nanostructure fabrication process.

Nanostructure Fabrication on Carbon Fabric

For the fabrication of the two nanostructure-coated electrodes, CNT growth on the carbon fabric was conducted using a plasma-enhanced chemical vapor deposition chamber (PECVD chamber) in which the plasma enhances CNT growth. Two nanoparticle layers were deposited on the carbon fabric in sequential steps as a bilayer on the carbon fabric: a 8.5-10 nm Al- underlayer functioning as a buffer, and a 1-2 nm Fe-catalyst layer that activated CNT growth. In order to prevent the oxidation of Al, the base pressure of the evaporation chamber was kept under 2×10^{-6} Torr; consequently, the bilayer was successfully fabricated without breaking the vacuum pressure; consequently, the bilayer was successfully fabricated without breaking the vacuum pressure.

The CNT growth on the carbon fabric in the PECVD chamber was carried out at 650-700 °C for 20 min. with 100 sccm CH_4 as a carbon source. A flow of 10 sccm of H_2 was introduced while heating and growing the CNTs; however, the effect of hydrogen was not dramatic in this growth condition. More amorphous carbon layers were formed at the outer walls of the CNTs without hydrogen. The chamber condition of the process was maintained at 800-mTorr-pressure, 320-W- power, with a 13.75 MHz RF plasma as an extra energy source to enhance CNT growth and to ensure that the growth was vertically-aligned.

The G-CNT-CF electrode was manufactured in two steps by using a thermal CVD chamber to prefabricate the graphene on the carbon fabric and by postfabricating the CNTs on the graphene-coated carbon fabric.

For the G-CNT growth on carbon fabric, the first step was the thermal evaporation of a 600 nm- Ni seed layer on the carbon fabric. The second step was to grow the graphene multilayers in a thermal CVD chamber.

Multiple layers of graphene growth were carried out in three steps by reducing the initial temperature of 960 °C to 840 °C, and finally reducing it to 800 °C for 5 min. with 1 sccm C_2H_2 as a carbon source; moreover, a flow of a-1 sccm H_2 was introduced while heating and growing the graphene layers. The chamber conditions of the process were maintained at 800-mTorr- pressure and 50 W- power.

Figure 1 shows a simple fabrication scheme for these two types of nanostructured carbon fabric.

Morphology and Surface Characterization of Nanostructured Carbon Fabrics

The microstructures of the carbon fabrics before and after the growth of the nanostructures were characterized using the field emission gun of a scanning electron microscope

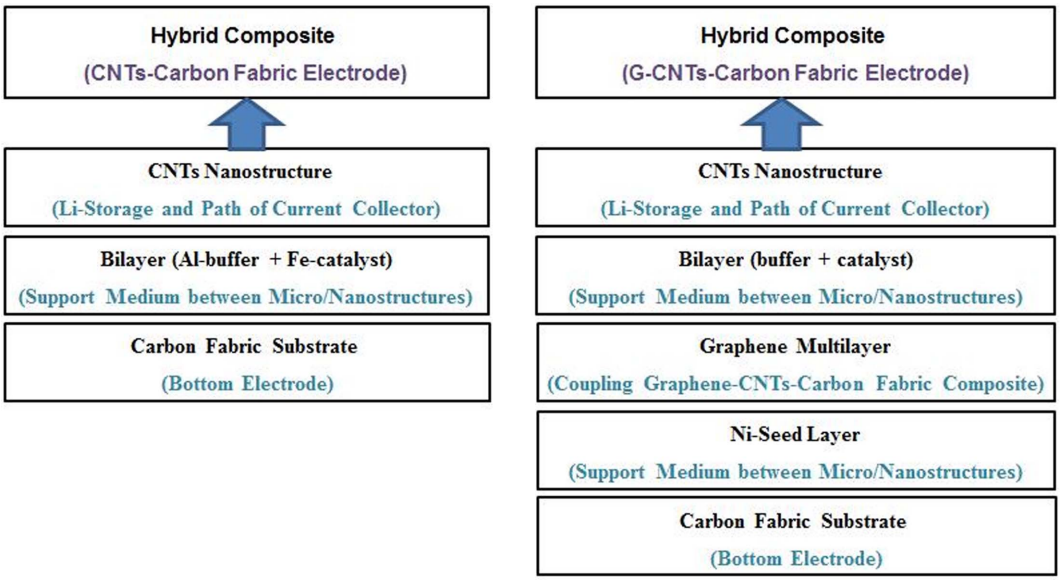

Figure 1. Scheme for the two types of nanostructured carbon fabric; (a) CNT growth step and (b) G-CNT growth step.

(FE-SEM) (S-4800, Hitachi), operating at 10 kV, without a conductive metal coating layer. For study of the interface between the VACNTs with graphene multilayers and the CF bottom electrode, multiple micro-scale samples were milled using an Ar-ion and a focused ion beam. Then, a field emission transmission electron microscope (FE-TEM) (Technai G^2F30 S-TWIN, FEI) and a field emission scanning transmission electron microscope (FE-STEM) (HD-2300A, Hitachi) were used for structural analysis of the nano-micro interfaces. Using Brunauer Emmett Teller (BET) and Barrett Joyner Halenda (BJH) methods, the specific surface areas and pore sizes of the nanostructured-CFs and pristine-CFs were investigated on an ASAP2020 (Micromeritics).

Chemical Characterization of Nanostructured Carbon Fabrics

The chemical structures of the nanomaterial coating were characterized using EA, ICP, XRD, and Raman spectra of the developed fabric electrodes to investigate material characteristics. The carbon content in the electrodes was determined by elemental analysis (Flash 2000, Thermo Scientific). Metallic elements such as Al, Fe, and Ni were determined by ICP optical emission spectrometer (Inductively Coupled Plasma testing machine, Thermo Scientific Co./ iCAP 6300 Duo). X-ray diffraction pattern of the developed fabric electrodes was confirmed by X-ray diffractormeter (XRD, D/MAX-RB 12 kW, Rigaku, Tokyo, Japan) with the wavelength of λ=0.15418 nm over the angular range of $10^{\circ} \leq 2\theta \leq 80^{\circ}$ at the step width of 0.01°. Raman spectroscopy was conducted with an ARAMIS from Horiba Jobin Yvon using argon ion laser excited at 514 nm.

Electrochemical Performance Testing

Galvanostatic cycling was performed on a battery cycler, WBCS3000S (Wonatech, Korea), and electrochemical impedance spectroscopy (EIS) was performed on an EC-Lab VMP 3 potentiostat/galvanostat (Biologic, France). To observe the lithiation and delithiation electrochemical phenomena in view of battery performance, electrochemical tests of half-cells for lithium ion batteries were assembled using a 2032-type coin cell. The charge/discharge characteristics of the samples were determined through cycling in the potential window of 0-2 V at 250 μA. The theoretical capacity of 372 $mAhg^{-1}$ for graphite was used to calculate the C-rate (372 mAg^{-1}=1 C-rate). Electrochemical impedance spectroscopy (EIS) was performed between 100 mHz and 1 MHz at the open circuit potential of the cell which had a signal peak-to-peak amplitude of 5 mV. For impedance spectroscopy, the ESR (Equivalent Series Resistance) was taken to be a real part of the impedance (Z_{real}) at a frequency of 1 kHz. Using this electrochemical test set-up, pristine-CF, CNT-CF, and G-CNT-CF were utilized as a working electrode in a lithium half-cell with lithium metal as a counter electrode. A porous glass fiber separator with a thickness of 1.55 mm was used. The electrolyte was a solution of 1 M LiPF6 and a mixture of ethylene carbonate and ethyle-methyle carbonate (EC-EMC) at a volume ratio of 1:1.

Results and Discussion

The Nanostructured Carbon Fabric

Table 1 summarizes the elemental analysis of carbon and metallic elements obtained using the pristine-CF, CNT-CF, and G-CNT-CF samples. Due to deposition of aluminum and iron nanoparticles as bi-layer in the process, the CNT-CF sample was observed to contain the abundant Al. and Fe. and to include the highest content of carbon of all the highly grown CNTs, while the G-CNT-CF sample was observed to included the lowest content of carbon. It can be assumed that the low carbon content of the G-CNT-CF is caused by surface ablation because the G-CNT-CF suffered a high temperature environment of more than 800 °C and up to nearly 1000 °C in the initial step of the CVD process. This means that the G-CNT-CF sample had to sacrifice a lot of carbon before the CNTs were grown.

Figure 2(a) shows X-ray Diffraction patterns (10-80 °) with marks of carbon and nickel of nanostructured carbon fabric; Figure (b) shows Raman spectrum of the pristine-CF, CNT-CF, and G-CNT-CF. A sufficient amount of Ni-. in the G-CNT-CF sample was observed in both the ICP and XRD patterns; this was due to the deposition of multiple Ni layers in the graphene growth process. Figure 2(a) shows that the (002) peak of the carbon material shifted gradually to the right. This means that the heat treatment condition of carbon materials can be affected by graphitic characteristics. The G-CNT-CF that was handled at the most highest temperature with the longest exposure showed the most graphitic behavior. The Raman spectra in Figure 2(b), with D/G band ratios of 1400-1600 cm^{-1} zone in indicates that stronger heat treatment condition can increase this ratio and, accordingly, amount of disordered carbon can be increased.

Nanostructured Carbon Fabric Morphology

The CNT-CF and G-CNT-CF nanostructured electrodes were successfully fabricated as shown in Figure 3. The rough surface of the carbon fabric led to different morphologies of the CNT-CF and G-CNT-CF surfaces.

Table 1. Elemental analysis and inductively coupled plasma results of Pristine-CF, CNT-CF, and G-CNT-CF

Sample	Elemental analysis (EA)	Inductively coupled plasma (ICP)		
	C (%)	Al (mg/kg)	Fe (mg/kg)	Ni (mg/kg)
Pristine-CF	94.621	192	301	31.5
CNT-CF	97.265	2.05×10^3	1.54×10^3	76.4
G-CNT-CF	73.494	407	634	3.33×10^4

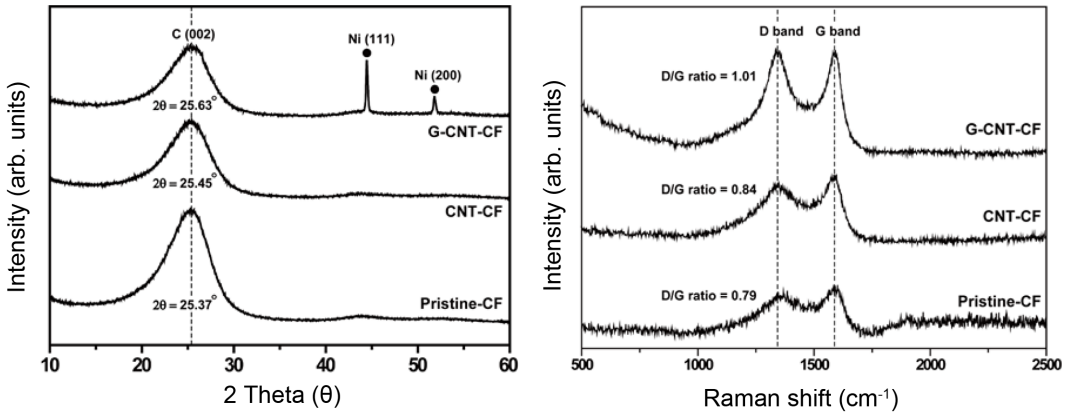

Figure 2. (a) X-ray Diffraction patterns (10-80 °) with marks of C and Ni and (b) raman spectrum of the pristine-CF, CNT-CF, and G-CNT-CF.

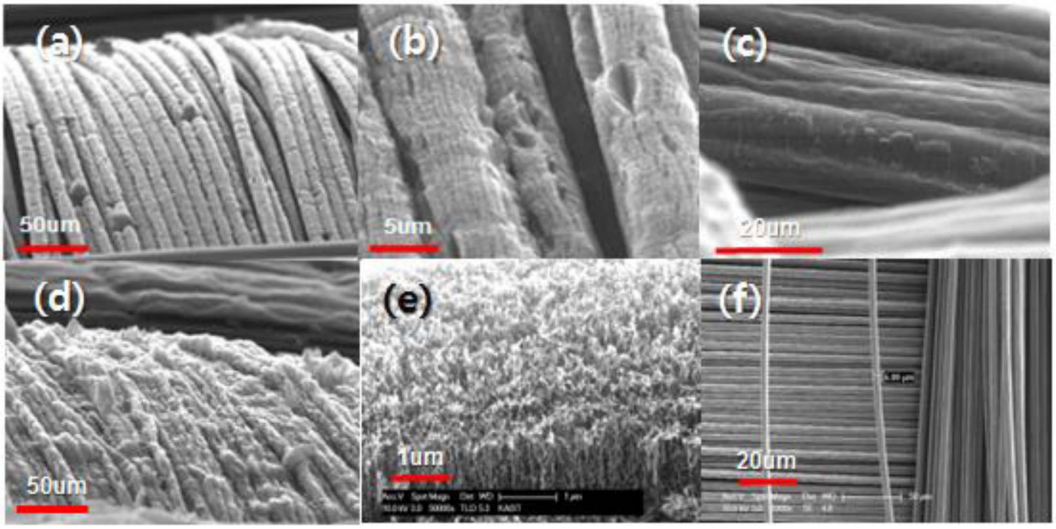

Figure 3. (a, b, c) SEM images showing the CNTs deposited on the carbon fabric, (d) G-CNTs deposited on the carbon fabric, (e) 50,000× magnification of CNTs deposited on the carbon fabrics, and (f) pristine carbon fabric.

Figures 3(a), (b), and (c) show the CNTs deposited on the carbon fabric; (d) shows the CNTs deposited on the graphene prefabricated carbon fabric at a tilted angle of 85 °. Figure 3(e) shows the CNT-CF at a tilted angle of 38 ° and 50,000x magnification. In magnified view, the surface morphology of the VACNT forest for G-CNT-CF was similar to that of CNT-CF. Figure 3(f) shows the base plane of the pristine carbon fiber surface.

In both the CNT-CF and the G-CNT-CF electrodes, high-yield- VACNTs were grown, but an undulating surface morphology of the VACNT forest for G-CNT-CF (Figure 3(d)) was observed, while the surface of CNT-CF was rather uniform (Figure 3(a)). Then, to better understand the micro-nanostructure interface, we observed the structural integrity of the cross-section area of the G-CNT-CF electrode.

The structural integrity of the G-CNT-CF electrode was analyzed utilizing multiple steps of microscopic observation. The microstructure of the cross-section area of the G-CNT-CF electrode was observed through low-power SEM and TEM imaging, while the nanostructure of the cross-section area was observed on a scanning transmission electron microscope (STEM) as shown in Figure 4(c)-(f). Figures 4(d)-(f) are the Secondary Electron (SE) image, High Angle Annular Dark Field (HAADF) image, and Transmission Electron (TE) image, with double magnification of the rectangle in Figure 4(c). In Figure 4(d), some portion of the Ni seed layer is anchored to the surface of the carbon fiber, while another portion has a certain gap from the carbon fiber surface in this cross-section. We can assume that the Ni seed layer with the gap in this cross-section can be a part of an Ni-overhang structure that stems from the carbon fiber surface in other locations along the carbon fiber. The surface-grown graphene and VACNT forest over the Ni seed layer in G-CNT-CF show the undulating surface morphology of the

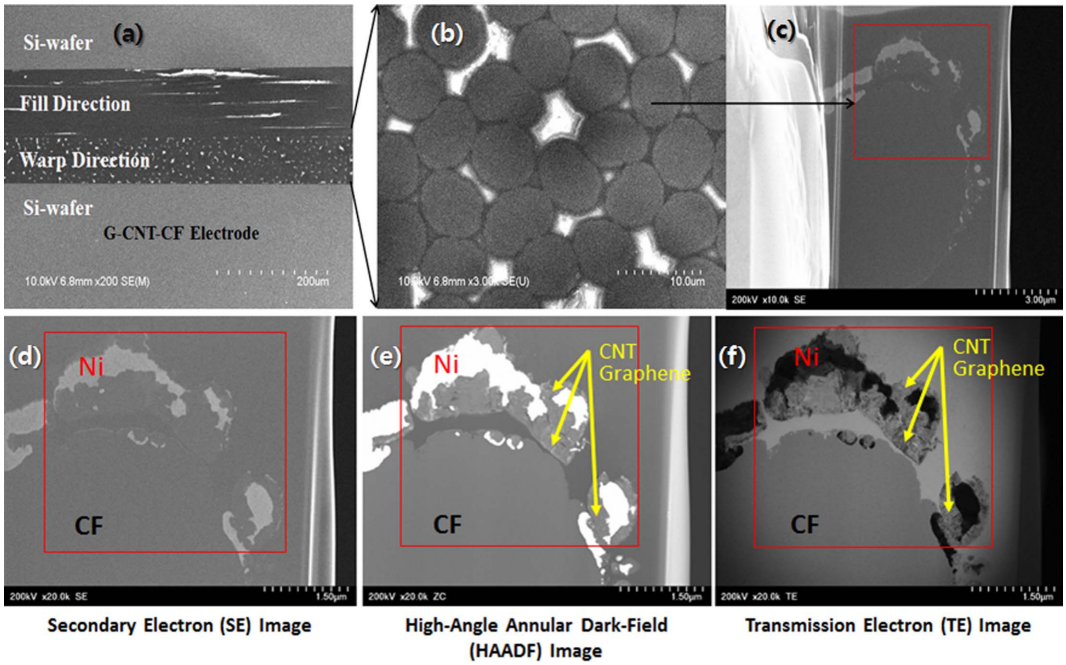

Figure 4. (a, b) SEM images showing G-CNTs deposited on carbon fabric and (c-f) STEM images showing G-CNTs deposited on carbon fabric. 600 nm Ni deposited as the underlayer for graphene growth while forming an overhang structure locally; 8.5 nm Al underlayer and 1.5 nm Fe catalyst layer for CNT growth.

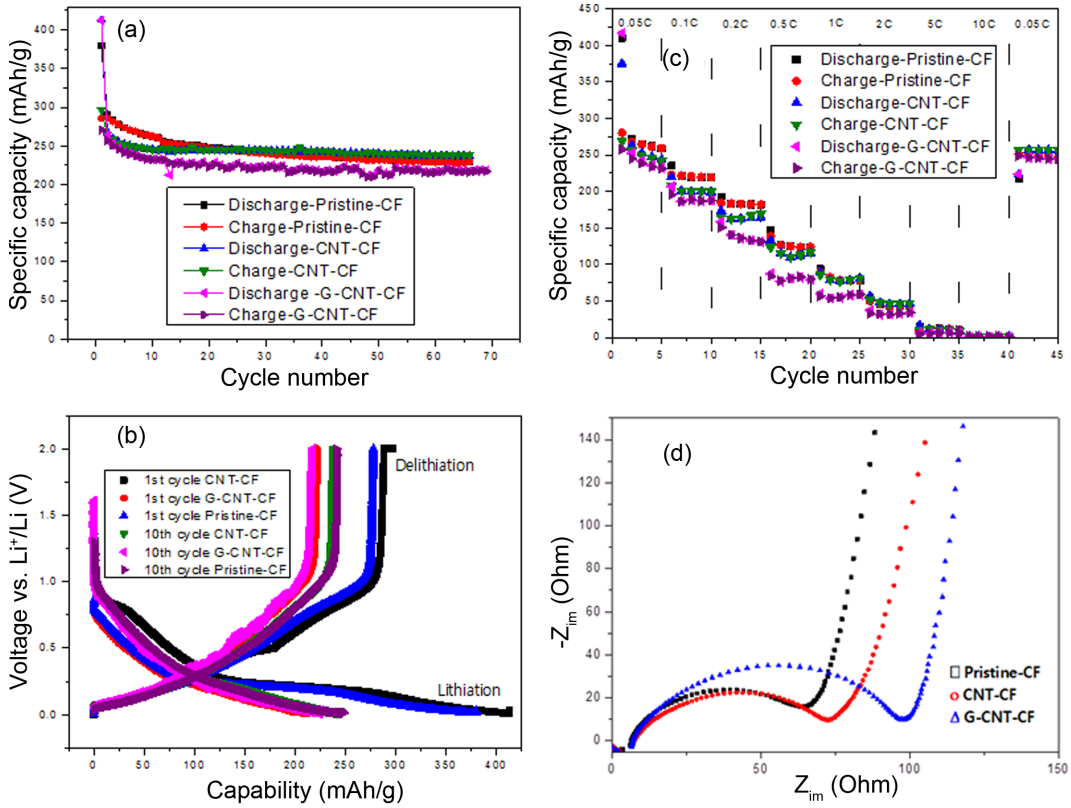

Figure 5. (a) Cyclic performance of CNT-CF, G-CNT-CF, and pristine-CF electrodes, (b) rate capability of CNT-CF, G-CNT-CF, and pristine-CF electrodes, (c) galvanostatic curves of CNT-CF, G-CNT-CF, and pristine-CF electrodes, and (d) EIS curves of CNT-CF, G-CNT-CF, and pristine-CF electrodes.

VACNT forest for G-CNT-CF (Figure 4(d)), while there is a rather uniform surface for CNT-CF (Figure 4(a)). This overhanging morphology may affect the G-CNT-CF electrode's electrical cyclic performance.

Battery Performance

The cyclic performance results at a-constant C-rate and at eight different C-rates are shown in Figure 5 and Figure 6, respectively. The CNT-CF electrode showed not only the best cyclic retention performance but also an excellent cycling performance from the tenth cycle onward.

BET results showed that the pristine-CF was 0.36 m^2/g; that of the and CNT-CF and G-CNT-CF were similar at 6.32 m^2/g. This may not seem a dramatic increase, but these results imply an advantage for battery applications due to the conventional carbon materials having a strong capacitive characteristic making them suitable for energy storage applications [15,16]. This dramatic increase of the specific surface area is important for the supercapacitor application, whereas our investigation is more concerned with the future of battery applications.

Cyclic Performance

In Figure 5(a), the galvanostatic cyclic performances of CNT-CF, G-CNT-CF and pristine-CF electrodes are presented for 66, 69, and 66 cycles, respectively, at a 0.05 C-rate.

In the total cycle life, including that represented by the galvanostatic curves in Figure 5(c), the reversible specific capacities of CNT-CF, G-CNT-CF, and pristine-CF electrodes were similar at about 250 mAh/g at a low current of 0.05 C-rate (C/20). The specific capacities after the tenth cycle of the pristine-CF, the CNT-CF, and G-CNT-CF electrodes were 265 mAh/g, 245 mAh/g, and 235 mAh/g, respectively. Although the performance during the first cycle may be attributable to the formation of a solid electrolyte interface (SEI), also known as the irreversible capacity, the first cycle's galvanostatic profile of the CNT-CF electrode was similar to that of the G-CNT-CF electrode.

Compared to the pristine CF, the relatively low capacity in G-CNT-CF or CNT-CF, considering their more than 17 times higher BET specific surfaces obtained by nano fiber grafting on the pristine CF, is due to the lack of aftertreatment of VACNT forest, such that wetting of the VACNT forest with electrolyte is insufficient. As such, the interstitial spaces of the VACNT forest cannot be fully accessed by the Li ions, even though the BET specific surfaces of G-CNT-CF and CNT-CF had much higher values of 6.32 m^2/g than pristine CF.

Rate Capability

In Figure 5(b), the cyclic retention of the CNT-CF electrode can be seen to have had the best initial performance (96 %),

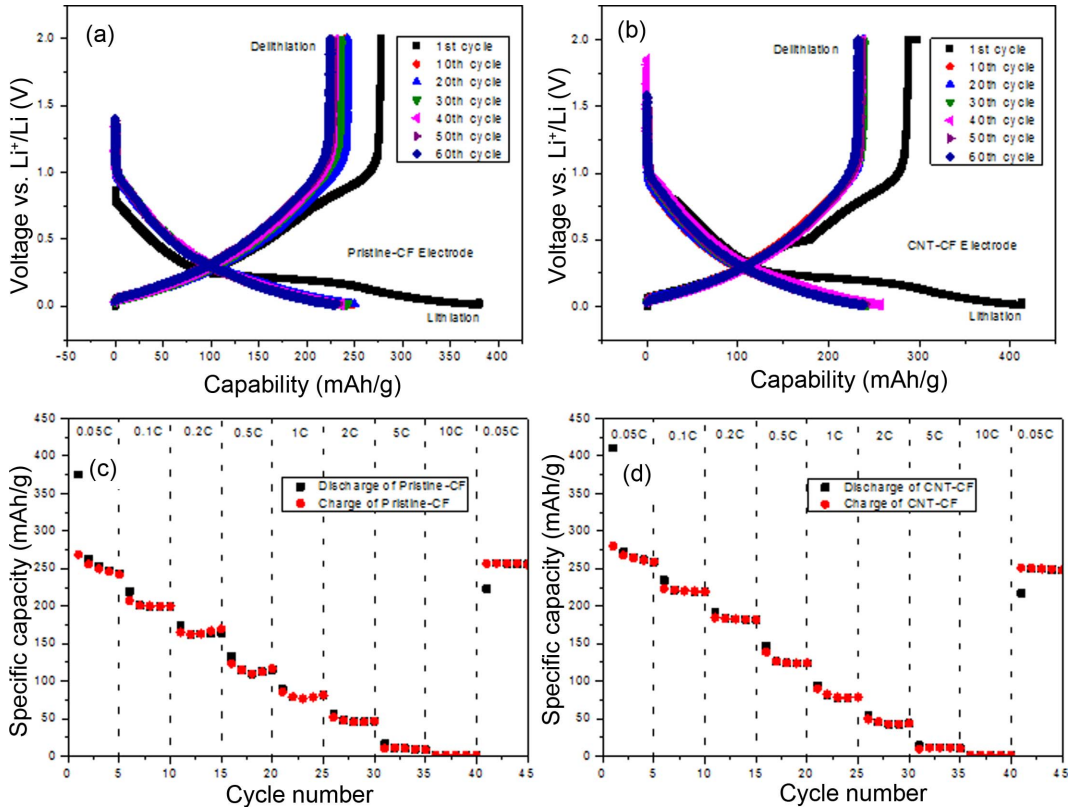

Figure 6. (a) Galvanostatic curves of pristine-CF electrode, (b) galvanostatic curves of CNT-CF electrode, (c) rate capability of pristine-CF electrode, and (d) rate capability of CNT-CF electrode.

while the pristine CF electrode showed a value of 86 % of initial performance. The G-CNT-CF electrode exhibited cyclic retention of 94 %. The CNT-CF electrode showed a perfect cyclic curve every 5 cycles from 0.05 C-rate up to 10 C-rate; the pristine-CF electrode showed a comparatively-constant cyclic curve every 5 cycles as well, while G-CNT-CF seemed to suffer cyclic degradation in most ranges. After terminating an initial cycling step from the 0.05 C-rate to the 10 C-rate condition, the second cycling at the 0.05 C-rate presented constant cyclic curves for all electrodes. This could be due to CF' hysteresis behavior; CNT and G-CNT, however, seemed to act as protective structures for the carbon fabric surface.

Electrochemical Impedance Spectra Curves

Electrochemical impedance spectra (EIS) curves of the pristine and the nanostructured CF electrodes were obtained to investigate the effects of the CNT-CF and G-CNT-CF electrodes on the electrical properties. Figure 5(d) shows an EIS profile consisting of a partially overlapped semicircle in the high frequency region that describes the charge transfer resistance (Rct), followed by a sloping line in the low frequency region, which could be considered as the Warburg impedance (Zw), associated with Li-ion diffusion in the bulk of the electrode [17,18]. Combining the diameters of the semicircles, it can be seen that the impedance of the CNT-CF electrode was smaller than that of the G-CNT-CF electrode; the impedance of the pristine-CF electrode was smaller than that of the CNT-CF electrode, showing this latter electrode's lower charge resistance.

New Perspectives on CNT-CF and Pristine-CF Electrodes for Structural Batteries

Figure 6 shows the new and competitive prospects of the pristine-CF and CNT-CF electrodes. In Figures 6(a) and (b), both galvanostatic charge-discharge curves show the cyclic performance of the specific capacity. Both electrodes have a similar potential window, but the OCV (Open Circuit Voltage) of the pristine-CF electrode is lower than that of the CNT-CF electrode for the given voltage of the 2 V in the galvanostatic experiment. After cycling, the pristine-CF electrode degraded gradually after the tenth cycle but the CNT-CF electrode had a-good capacity retention of nearly 99 % between the 10th and 50th cycles. Figures 6(c) and (d) show the rate capability curves according to the varying C-rate conditions every 5 cycles. After galvanostatic charge-discharge behaviors were terminated, the second 0.05 C-rate charge-discharge performance showed a perfect recovery of capacity retention. Therefore, it can be proven that, in an acidic environment, pristine-CF and CNT-CF electrodes maintain their capacity retention, during their long lifecycles.

Considering the CNT-CF electrode's non-sacrificial characteristic under electrochemically severe conditions, this result suggests that the combination of CNT and CF functions as an effective barrier to protect the carbon fabric surface from electrochemically severe acidic environments. This perspective enables an expectation that the CNT-CF electrode has great potential as a structural battery electrode because a key necessity for an electrochemically long-lasting battery application is that it has a longer cycle life, while carbon material is known to have strong capacitive behavior and to exhibit hysteresis.

Conclusion

We have fabricated MWCNT-grown carbon fabric electrodes from methane using CVD at 650-700 °C. Ion beam sputtering was used to sequentially deposit an Al- underlayer and a Fe-active catalyst layer on a carbon fabric surface. Optimization of these two layers was accomplished to grow densely- and vertically-aligned MWCNTs. This approach of using an Al-underlayer for CNT growth on a rough surface of carbon fabric may work very well because the underlayer functions as a strong binding between the incompatible combination of the catalyst metal layer and the carbon fabric substrate and also because having an underlayer protects the amorphous carbon fabric from unexpected damage by preventing excessive catalyst metal layer deposition on the carbon fabric substrate.

Through this approach of growing CNTs on carbon fabric, we have provided a new perspective on commercially-available continuous carbon fabric for the energy-storage structure of structural battery electrodes. Even though the capacity of VACNT-grafted carbon fabrics was limited due to poor wetting of the VACNT forest with electrolyte, caused by lack of functionalization of VACNT, the excellent cyclic performances and galvanostatic curves support the idea that a carbon nanotube and carbon fabric combination can be utilized in structural battery applications in future research. While this nanostructured CNT-CF is an effective concept for energy storage applications, pristine carbon fabric is still a good candidate due to its comparative ease of handling. Since multifunctional applications of carbon fabric-based electrode materials, such as energy-storage structures, are still very attractive due to their lightweight and load-bearing strength, this area is not an emerging field but a mature technological one in aerospace, automotive, and high-efficiency advanced systems and devices that demand multifunctionality.

Acknowledgements

This work was supported by the Agency for Defense Development (ADD) as a part of the Basic Research Program under contract UD130049GD, and by a National Research Foundation of Korea (NRF) grant funded by the Korean government (MSIT) (No. 2017R1A2B2010148). The authors gratefully acknowledge the assistance in the preparation of nanostructured specimens of the Center for Thin Film Materials of the Korea Research Institute of Chemical

Technology and the Department of Nano-Structured Materials Research of the National Nanofab Center.

References

1. Y. Gao, S. P. Adusumilli, J. Turner, L. Lesperance, C. Westgate, and B. Sammakia, *J. Nanosci. Nanotechnol*., **12**, 10 (2012).
2. S. Park, D. W. Park, C. S. Yang, K. R. Kim, J. H. Kwak, H. M. So, C. W. Ahn, B. S. Kim, H. Chang, and J. O. Lee, *ACS Nano*., **5**, 9 (2011).
3. Y. Gao, G. P. Pandey, J. Turner, C. R. Westgate, and B. Sammakia, *Nanoscale Res. Lett*., **7**, 651 (2012).
4. J. Li, Q. Ye, A. Cassell, H. T. Ng, R. Stevens, J. Han, and M. Meyyappan, *Appl. Phys. Lett*., **82**, 15 (2003).
5. X. Shui and D. D. L. Chung, *J. Power Sources*, **47**, 313 (1994).
6. D. T. Welna, L. Qu, B. E. Taylor, L. Dai, and M. F. Durstock, *J. Power Sources*, **196**, 1455 (2011).
7. L. Delzeit, C. V. Nguyen, B. Chen, R. Stevens, A. Cassell, J. Han, and M. Meyyappan, *J. Phys. Chem. B*, **106**, 22 (2002).
8. M. J. Behr, E. A. Gaulding, K. A. Mkhoyan, and E. S. Aydil, *J. Appl. Phys*., **108**, 053303 (2010).
9. K. C. Pham, D. H. C. Chua, D. S. McPhail, and A. T. S. Wee, *ECS Eletrochem. Lett*., **3**, 6 (2014).
10. H. Qian, A. R. Kucernak, E. S. Greenhalgh, A. Bismarck, and M. S. P. Shaffer, *ACS Appl. Master. Inter*., **5**, 6113 (2013).
11. S. Leijonmarck, T. Carlson, G. Lindbergh, L. E. Asp, H. Maples, and A. Bismarck, *Compos. Sci. Technol*., **89**, 149 (2013).
12. J. K. Lee, K. W. An, J. B. Ju, B. W. Cho, W. I. Cho, D. Park, and K. S. Yun, *Carbon*, **39**, 1299 (2001).
13. M. H. Kjell, E. Jacques, D. Zenkert, M. Behm, and G. Lindbergh, *J. Electrochem. Soc*., **158**, 12 (2011).
14. E. Pamula and P. G. Rouxhet, *Carbon*, **41**, 1905 (2003).
15. A. L. M. Reddy, F. E. Amitha, I. Jafri, and S. Ramaprabhu, *Nanoscale Res Lett*., **3**, 145 (2008).
16. K. Jost, C. R. Perez, J. K. McDonough, V. Presser, M. Heon, G. Dion, and Y. Gogotsi, *Energ. Environ. Sci*., **4**, 5060 (2011).
17. S. Moon, Y. H. Jung, and D. K. Kim, *J. Power Sources*, **294**, 386 (2015).
18. P. R. Kumar, Y. H. Jung, and D. K. Kim, *RSC Adv*., **5**, 79845 (2015).